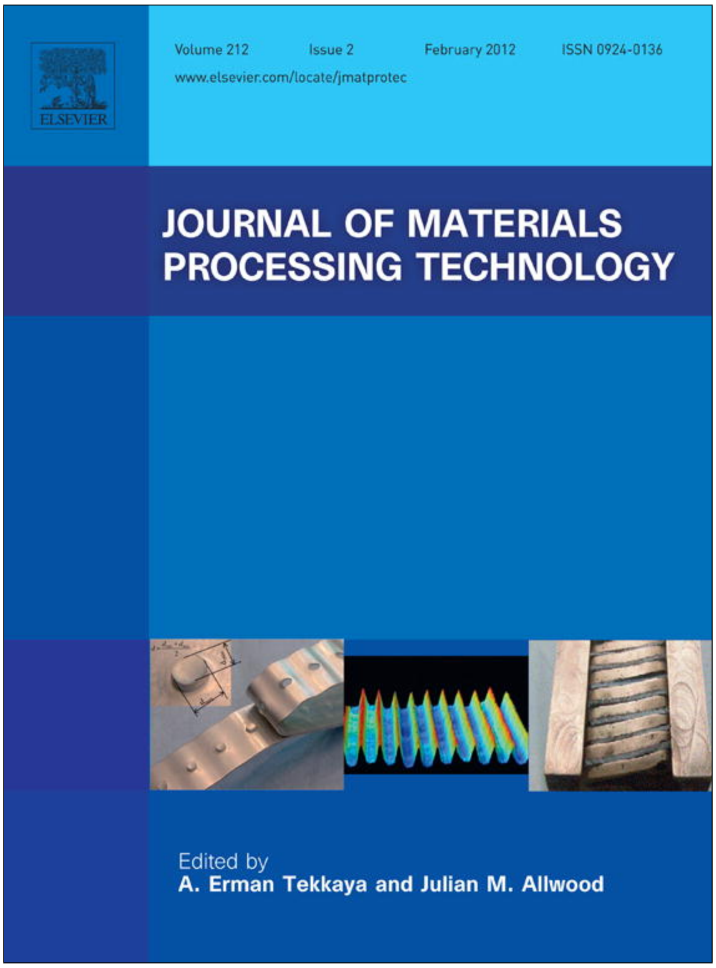
Volume 212
Issue 2
February 2012
ISSN 0924-0136
www.elsevier.com/locate/jmatprotec
ELSEVIER
JOURNAL OF MATERIALS PROCESSING TECHNOLOGY
Edited by
A. Erman Tekkaya and Julian M. Allwood

Journal of Materials Processing Technology 212 (2012) 509–515

Contents lists available at SciVerse ScienceDirect

Journal of Materials Processing Technology

journal homepage: www.elsevier.com/locate/jmatprotec

Analysis of texture and *R* value variations in asymmetric rolling of IF steel

Laszlo S. Tóth[a,*], Benoit Beausir[b], Dmitry Orlov[c], Rimma Lapovok[c], Arunansu Haldar[d]

[a] Laboratoire d'Etude des Microstructures et de Mécanique des Matériaux, CNRS UMR 7239, Université Paul Verlaine – Metz, Ile du Saulcy, 57045-METZ Cedex 01, France
[b] Institut für Strukturphysik, Technische Universität Dresden, D-01062 Dresden, Germany
[c] ARC CoE for Design in Light Metals, Materials Engineering Department, Monash University, Clayton, Victoria 3800, Australia
[d] R&D Division, Tata Steel Ltd., Jamshedpur 831001, India

ARTICLE INFO

Article history:
Received 12 May 2011
Received in revised form 5 August 2011
Accepted 19 October 2011
Available online 25 October 2011

Keywords:
IF steel
Asymmetric rolling
Ideal orientations
Texture
R value
Polycrystal modelling

ABSTRACT

Asymmetric rolling (ASR) is a potential process to reach better grain refinement than in conventional rolling, thus, can lead to better mechanical properties. It is not known, however, how the introduction of a shear component will change the ideal orientations of the textures, and consequently, the evolution of plastic anisotropy. To understand the effect of the added shear on texture evolution in ASR, a stability analysis is carried out in orientation space and the variations in the position and strength of the ideal orientations are analysed as a function of the shear component. Then, modelling of *R* values is presented for various cases. On that basis, it is shown that there is an upper limit for the shear component in asymmetric rolling that still retains the ⟨1 1 1⟩ || ND fibre (ND: direction normal to the sheet) which is good for formability. It is also found that better persistence of the ND fibre can be obtained by cyclically alternating the shear component. The theoretical results are well supported by comparison to experimental evidences.

1. Introduction

As comprehensively reviewed by Takechi (1994), interstitial free (IF) steel is an important industrial product that presents large plastic deformation capacities. Its good formability originates from its strong ND fibre (⟨1 1 1⟩ || ND). Urabe and Jonas (1994) demonstrated that an ND fibre can be produced by suitable thermo mechanical processing. Takechi (1994) also highlighted that one disadvantage of IF steel is its relatively low strength (ranging from about 100 MPa to max. 350 MPa) due to the low alloying content which is only used to stabilize C and N. It is therefore important to seek deformation processes that might improve the strength of IF steel while maintaining its good formability.

As can be concluded from the works of Kocks and Mecking (2003) and Meyers et al. (2006), a possible way to improve material strength is Hall-Petch type strengthening through the reduction of the average grain size. There is an increasing research in the field of severe plastic deformation (SPD) processes which shows that very large plastic strains can refine the microstructure very efficiently producing ultrafine grained (UFG) materials; see for instance the comprehensive review by Azushima et al. (2008) about the effects of SPD processing on metals. Among them, the most widely studied techniques are equal channel angular extrusion (ECAE) introduced by Segal et al. (1981) and reviewed by Valiev and Langdon (2006), high pressure torsion (HPT) recently reviewed by Zhilyaev and Langdon (2008), and accumulative roll bonding (ARB) introduced by Tsuji et al. (1999). New techniques for severe plastic deformation are also emerging. One can mention for example; twist extrusion invented by Beygelzimer et al. (2002) and thoroughly studied by Orlov et al. (2009), or a more recent technique proposed by Tóth et al. (2009) in which tubes are twisted under high hydrostatic pressure. These techniques greatly expand the capabilities of SPD processes for rod and tube UFG products manufacturing, respectively. For sheet processing, one of the best candidates is asymmetric rolling (ASR). As reviewed by Salganik and Pesin (1997), ASR requires the minimum changes in a rolling line. According to the classification by Gorelik and Klimenko (1997), it can be done in various ways: one can do ASR with different roll diameters, different angular speeds of the rolls, assuring different frictions on the two sides of the sheet, or simply by leaving one of the rolls idle. In an analytical model of ASR developed by Potapkin et al. (1987) with one roll idle it was shown that the heterogeneity of stress and strain states along the sheet height does not exceed 8%. In a later work, presented by Richelsen (1997) using final-element (FE) modelling with differential friction a non-monotonic dependence of the sheet curvature on height reduction was found. A FE model and a control system for ASR was developed by Dyja et al. (1994) and implemented in industrial conditions. It allowed

* Corresponding author. Tel.: +33 3 87 31 53 61; fax: +33 87 31 53 66.
E-mail addresses: Toth@univ-metz.fr (L.S. Tóth), benoit.beausir@univ-metz.fr (B. Beausir), dmytro.orlov@monash.edu (D. Orlov), rimma.lapovok@monash.edu (R. Lapovok), arunansuhaldar@tatasteel.com (A. Haldar).

0924-0136/$ – see front matter © 2011 Elsevier B.V. All rights reserved.
doi:10.1016/j.jmatprotec.2011.10.018

achieving improvement in sheet shape quality and an increase of the production output. In the above mentioned works and even in a more recent work presented by Ji and Park (2009), only technological aspects affecting the rolling process parameters and the effects of ASR on the shape of the rolled sheet was considered. Comparisons of these processes in terms of materials microstructure, texture and evolution of mechanical properties have been recently examined by various authors. For example, Apps et al. (2004) carried out a comparative analysis between ECAE, ARB and ASR for the production of high strain-rate superplastic alloys; Lapovok et al. (2009) investigated the differences obtained by ECAE and ASR for aluminium alloy 6111, and Orlov et al. (2010) analysed ASR of IF steel.

In the present work, asymmetric rolling of IF steel is studied in comparison with conventional rolling. The objective is to examine the characteristics of the ideal crystal orientations together with the variations in the texture during ASR. As the ideal orientations for ASR have not been identified yet, first a theoretical study was carried out using an orientation stability analysis. The present analysis is based on an earlier work of Tóth et al. (1990) carried out for ferrite textures in SR which was recently generalized by Tóth (2008) for textures in other materials during plastic deformation in different modes. As an application, the ideal ND fibre was selected in this work to study the effects of ASR on the development of the texture. R values were also calculated using the viscoplastic self-consistent polycrystal model (VPSC) and were compared to measured values.

2. Basic definitions of orientation stability

In the present analysis, the velocity field in orientation space corresponding to the orientation changes that can take place during SR and ASR are analysed using the technique proposed by Tóth et al. (1988) and further developed by Arzaghi et al. (2009). An orientation is identified by its Euler angles which is a vector in orientation space: $\vec{g} = (\phi_1, \phi, \phi_2)$. Orientations can move during plastic strain; their velocity is given by the vector $\dot{\vec{g}} = (\dot{\phi}_1, \dot{\phi}, \dot{\phi}_2)$. $\dot{\vec{g}}$ can be obtained from crystal plasticity using, for example, viscoplastic slip and the Taylor mode of deformation. $\dot{\vec{g}}$ strongly depends on the strain mode and the available slip systems. For IF steel, the $\{1\,1\,0\}\langle 1\,1\,1\rangle$ and $\{1\,1\,2\}\langle 1\,1\,1\rangle$ slip families were used in the present work with a relative strength of flow resistance of 0.95 where the $\{1\,1\,2\}$ slip is easier. The preference for $\{1\,1\,2\}$ slip was supported by the findings reported by Daniel and Jonas (1990). $m = 0.05$ was used for the exponent of the strain rate sensitivity of viscoplastic slip using the constitutive law for slip that had been proposed by Hutchinson (1976).

The stability of a texture component requires that the rotation speed vanishes; $\dot{\vec{g}} = (\dot{\phi}_1, \dot{\phi}, \dot{\phi}_2) = 0$, or at least sufficiently low (it can be exactly zero in the ideal orientations of rolling, however, it is a small non-zero value in simple shear). The other, equally important requirement is that more grain orientations are coming in than leaving from a near ideal position, which can be expressed by the divergence quantity:

$$div\dot{\vec{g}} = \frac{\partial\dot{\phi}_1}{\partial\phi_1} + \frac{\partial\dot{\phi}}{\partial\phi} + \frac{\partial\dot{\phi}_2}{\partial\phi_2} < 0 \quad (1)$$

The variations in the ODF intensities f can be described by the Eulerian equation of orientation density evolution which was first proposed by Clément and Coulomb (1979) and was used later by Gilormini et al. (1990) to predict the ODF in an analytic way in the following form:

$$(\dot{f}/f)_g = -\dot{\phi}\cdot\cot\phi - div\,\dot{\mathbf{g}} - \dot{\mathbf{g}}\cdot grad(\ln(f)) \quad (2)$$

Here the $\dot{\phi}\cot\phi$ quantity is originating from the distortion of Euler space. It is clear that for increasing ODF intensity, the divergence has to be negative if the last term in Eq. (2) can be neglected. It was shown by Tóth et al. (1990) that for rolling textures, the ideal orientations are actually located within negative divergent regions of Euler space. However, for simple shear textures, it was shown by Tóth et al. (1988) for f.c.c. crystals that the ideal orientations are such that the divergence changes sign at their exact location. Arzaghi et al. (2009) have confirmed this finding for b.c.c. crystals. The $\dot{\mathbf{g}}\cdot grad(\ln f)$ can play an important role only when strong texture is formed. In the following, two quantities will be used to examine the persistence characteristics of a texture component; the lattice rotation rate vector and the divergence quantity. As $\dot{\mathbf{g}}$ is a vectorial quantity, for the purpose of our stability analysis its absolute value will be used. From $\dot{\mathbf{g}}$, the lattice spin vector $\vec{\Omega}$ can be readily calculated (see the equations in Tóth et al., 1988), then a persistence parameter P can be defined from it. In the present work we use the definition of P proposed by Arzaghi et al. (2009):

$$P(g, \dot{\varepsilon}) = 1 - \left[\frac{|\Omega(g, \dot{\varepsilon})|}{\Omega_{\max}}\right]^{1/3} \quad (3)$$

Here $|\Omega| = \sqrt{\Omega_{12}^2 + \Omega_{31}^2 + \Omega_{23}^2}$ is the absolute value of the lattice spin and $\Omega_{\max}$ is the maximum value of it in the whole Euler space for the given deformation mode defined by the strain rate tensor $\dot{\varepsilon}$. The exponent 1/3 in Eq. (3) was chosen so that a plot of the persistence parameter resembles to an ODF of a well-deformed material. P varies between 0 and 1. Note that a different definition for P – proposed by Tóth et al. (1988) – was used in previous works: in the work for shear of hexagonal crystals by Beausir et al. (2007) and in Tóth et al. (1990) for shear and rolling of b.c.c. crystals. That definition had a problem of division by zero for perfectly ideal orientations. The advantage of the present formula (Eq. (3)) is that it can never lead to singularities.

3. Persistence characteristics of the textures during symmetric and asymmetric rolling

As presented in Section 2 above, the relevant quantities for the persistence behaviour of textures are the divergence quantity (Eq. (1)) and the P parameter defined by Eq. (3). They were calculated in Euler space on a 3° grid using the full constraints crystal plasticity model, i.e., the Taylor model. The imposed deformation mode was defined by the following velocity gradient increment and the corresponding strain tensor increment:

$$d\underline{\underline{L}} = \begin{bmatrix} d\varepsilon & 0 & sd\varepsilon \\ 0 & 0 & 0 \\ 0 & 0 & -d\varepsilon \end{bmatrix}, \quad d\underline{\underline{\varepsilon}} = \begin{bmatrix} d\varepsilon & 0 & sd\varepsilon/2 \\ 0 & 0 & 0 \\ sd\varepsilon/2 & 0 & -d\varepsilon \end{bmatrix} \quad (4)$$

Eq. (4) describes a plane strain deformation mode, which is usually used as an approximation for rolling. The shear component that is introduced by ASR is a simple shear in the plane of rolling and in the direction of rolling. Here the shear increment is $sd\varepsilon$ with s being the shear coefficient characterizing the contribution of the shear with respect to the rolling strain (negative s values will be also considered here). Such approximation of the ASR process was already used in Beausir et al. (2009). A more general description of the strain field was developed by Beausir and Tóth (2008) for ASR and by Beausir et al. (2005) for SR using a flow line approach.

The existence of ideal components for ASR has not yet been examined before neither theoretically or experimentally. Nevertheless, it can be expected that they exist. The following arguments can be forwarded to support this statement. For symmetric rolling, the ideal components are well known, also for the case of simple shear. The ASR deformation mode lies between these two well-established deformation modes so the ideal orientations that correspond to ASR should be situating between those of symmetric rolling and simple shear. One could also argue that the deformation tensor in Eq. (4) could be expressed in a rotated reference system so that it contains only two diagonal components, just like in symmetric rolling (when it is approximated by plane strain) for which case ideal orientations do exist. Thus, in the following, the orientation stability analysis presented above will be applied for the case of ASR to explore the exact nature of the expected ideal textures.

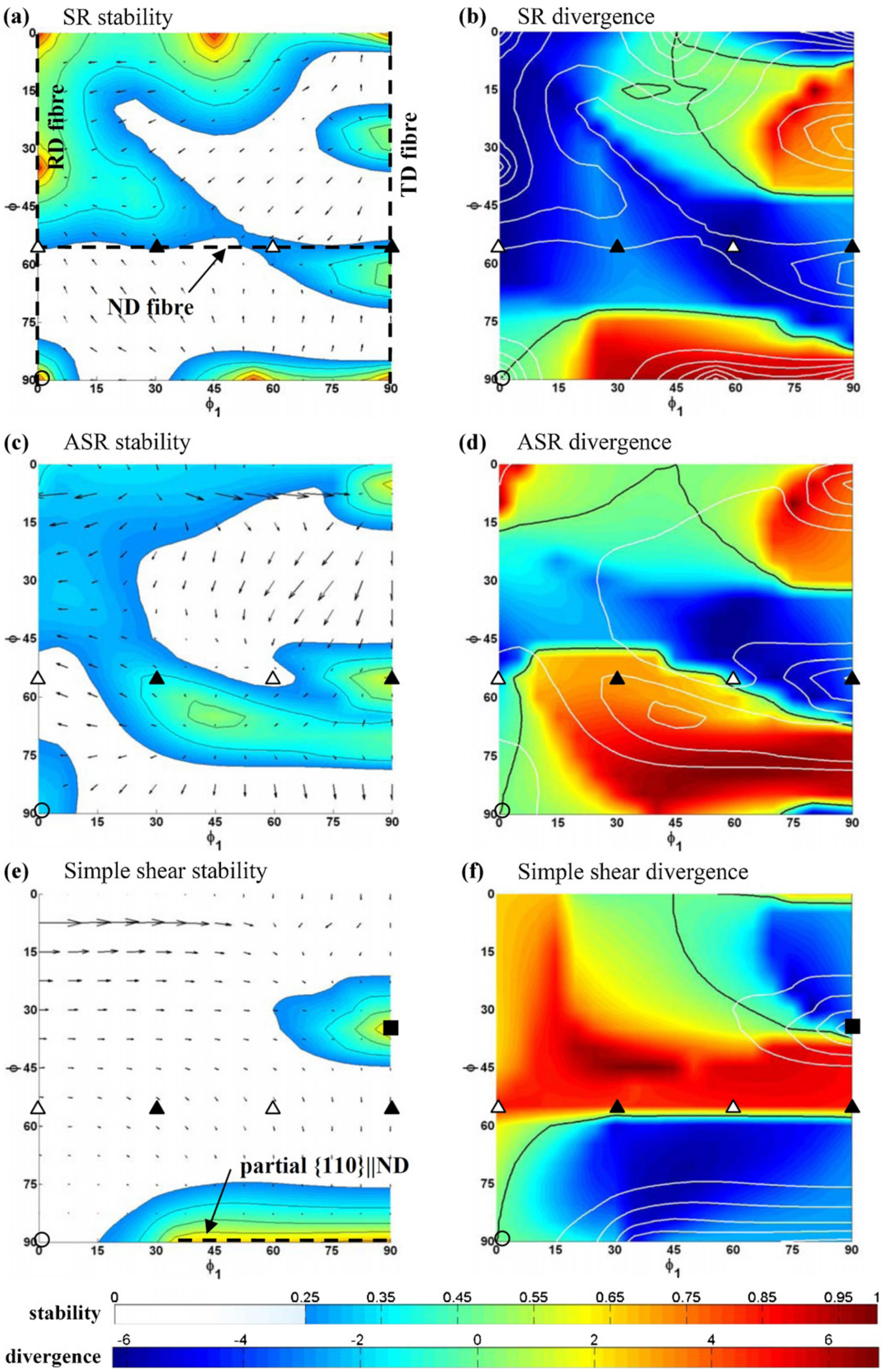

Fig. 1. $\varphi_2 = 45^\circ$ section of Euler space displaying the stability parameter P (a, c and e) and the divergence (b, d and f) for symmetric rolling, asymmetric rolling and simple shear, respectively. The colour code for the iso-intensities are also shown; the upper one for P, the lower one for the divergence. Symbols locate the following ideal orientations: (○) (1 1 0)[1 $\bar{1}$ 0], (△) (1 1 1)[1 $\bar{1}$ 0] and (1 1 1)[0 $\bar{1}$ 1], (▲) (1 1 1)[1 $\bar{2}$ 1] and (1 1 1)[$\bar{1}$ $\bar{1}$ 2], (■) D (1 1 2)[$\bar{1}$ $\bar{1}$ 1].

In the following, only the $\varphi_2 = 45^\circ$ section of the orientation space will be shown here as this section contains all major orientations of rolling textures (for a key figure of the ideal orientations for rolling of bcc metals, see in Tóth et al., 1990). Three cases are presented in this paper: symmetric rolling; $s = 0$, asymmetric rolling with a shear contribution of $s = 1$ and simple shear; $s \gg 1$.

Fig. 1a displays the stability map together with the projection of the rotation field for symmetric rolling. The ideal orientations have to be located in regions with high intensity of P. One can see that large part of the RD fibre has high P values. Concerning the ND fibre; it appears in distorted/rotated form. There are also local maximum P regions where ideal orientations are not expected. This is why it is important to plot the divergent quantity as well, see Fig. 1b. The blue areas represent negative divergences in Fig. 1b where the iso-contours (in white colour) of the stability parameter P are also superimposed. In the red areas the divergence is positive, thus, no ideal orientations are expected in those regions even if the P parameter is high. Fig. 1b clearly shows the stability of the RD and ND fibres as well as orientations that are located between the cube and the rotated cube. Actually, experimental ODFs of rolling textures have characteristics very similar to Fig. 1b.

For asymmetric rolling, when the shear value is equal to the rolling strain ($s = 1$), the situation is substantially different, see Fig. 1c and d. The main feature is that the ND fibre is displaced down towards larger ϕ angles. At the same time, at low ϕ angles, on the top part of the map, there is no stability in the vicinity of the cube and rotated cube orientations. When looking at the divergence map, one can see that the blue areas moved as well, however, in the opposite direction with respect to the P-map. The combined result is that the stability along the ND fibre is limited to the large ϕ angles near the $(1\,1\,1)[\bar{1}\,\bar{1}\,2]$ orientation while the RD fibre is strong only at $(1\,1\,2)[\bar{1}\,\bar{1}\,0]$. Note that because of the presence of the shear component, the orthotropic symmetry is not valid in ASR, thus, in principle, the Euler space should be doubled in the φ_1 direction. Nevertheless, for comparison purposes, the reduced space is also suitable here. The only important fact is that no orthotropic symmetry should be applied in measured or simulated ODFs for asymmetric rolling.

The extreme case of ASR is when the shear component is so high that the rolling strain can be neglected and the strain state becomes simple shear. That situation is displayed in Fig. 1e and f. It is clear that both the RD and ND fibres are completely unstable for simple shear. In the Euler angle range presented in Fig. 1, one can identify the D ideal orientation and the partial $\{1\,1\,0\} \,||$ ND fibre which are typical components of bcc shear textures, see a complete presentation of all ideal orientations for bcc shear in orientation space by Baczynski and Jonas (1998) and in pole figures by Montheillet et al. (1985). It can be seen in Fig. 1 that for the case of simple shear the ideal orientations are located along the border line that separates positive and negative divergence areas. This is characteristic to shear deformation and was also pointed out by Tóth et al. (1988) for shear of f.c.c. crystals.

4. Texture variations of the ideal ND fibre during symmetric and asymmetric rolling

IF steel is mainly produced because its good formability due to its strong ND fibre. Suitable rolling and subsequent recrystallization permits the development of a very pronounced ND fibre. It is therefore important to know, how such a fibre develops during symmetric/asymmetric rolling. For this purpose, polycrystal simulations were carried out using both the Taylor and VPSC models starting from an ideal ND fibre. For the VPSC approach, the version tuned by Molinari and Tóth (1994) was employed. The initial ideal texture consisted of 4000 orientations after applying orthotropic symmetry on the initial 1000 grain orientations. Such a symmetrization is necessary before ASR (recall that it cannot be applied *after* ASR as it was discussed above). Strain hardening was not modelled as it usually has small effect on texture development. The initial texture is shown in Fig. 2. Its maximum intensity along the ideal fibre was 6.5. The textures obtained from the Taylor and VPSC models are also displayed in Fig. 2. The applied strain was $\varepsilon = 1$ in the SR and ASR cases while a shear of $\gamma = 2$ was applied for the case of simple shear. As can be seen in Fig. 2, the texture develops precisely as predicted from the stability analysis in Section 3 above in the case of the Taylor model. However, the VPSC model prediction is significantly different. For the SR and ASR cases, it produces

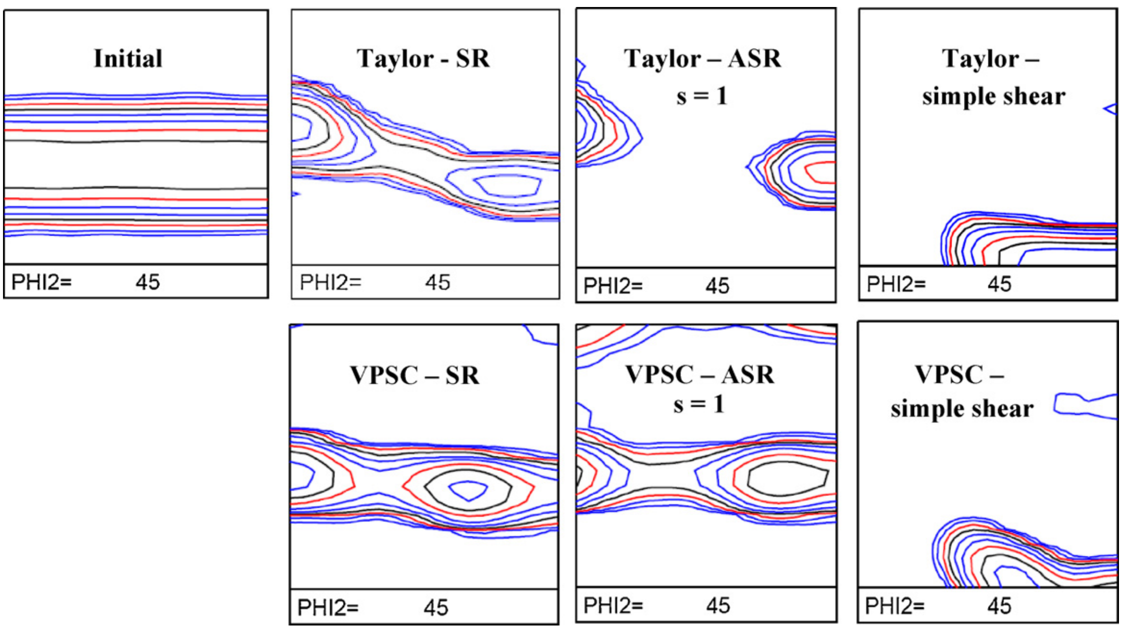

Fig. 2. Textures developing from an initial ideal ND fibre during symmetric and asymmetric rolling as well as during simple shear using the Taylor and VPSC polycrystal models. Isolevels: 0.8, 1.3, 2, 3.2, 5, 8, 13, 20, 32.

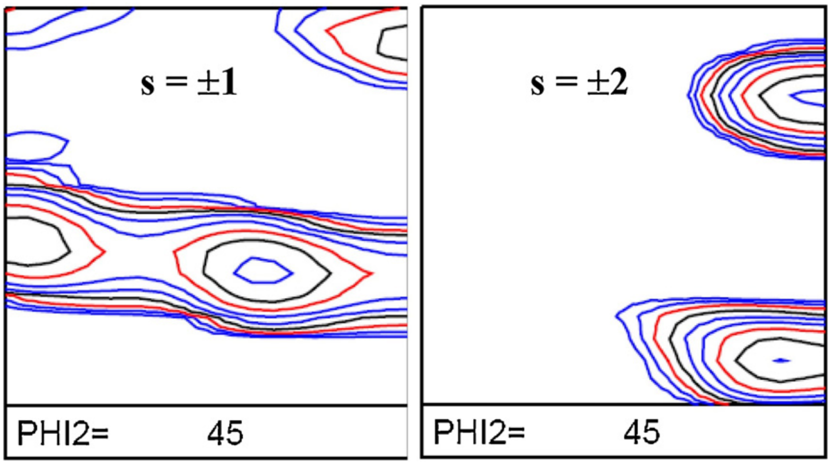

Fig. 3. ASR simulated textures obtained with the VPSC model by alternating the sign of the shear component. The initial texture was ideal ND fibre. Isolevels: 0.8, 1.3, 2, 3.2, 5, 8, 13, 20, 32.

a continuous ND fibre nearly in its ideal position, even for the ASR case. It should be noted, however, that for larger shear components than $s = 1$, the ND fibre disappears (not shown to save space), only the $(1\,1\,1)[\bar{1}\,\bar{1}\,2]$ component survives. Actually, the VPSC model is in better agreement with experiments as will be shown below. The ND fibre further strengthens during symmetric rolling and remains in position. It was not known, however, that this fibre can be maintained also during ASR, even for large proportions of shear.

Simulations were also carried out for the case when the shear component is changing sign between successive passes of ASR. The results obtained with the self-consistent model for $s = \pm 1$ and $s = \pm 2$ are shown in Fig. 3. In both cases the rolling strain was $\varepsilon = 1$. For the simulation in the $s = \pm 1$ case, two passes were applied (one 'cycle') while for $s = \pm 2$, there were four passes (two 'cycles'). As can be seen, the ND fibre is maintained – and it is even strengthened with respect to the monotonic case – when $s = \pm 1$. However, for $s = \pm 2$, the ND fibre disappears.

In order to understand the evolution of the texture for the cycling ASR case, the rotation field together with the stability parameter P and the divergence is plotted for the $s = -1$ case in Fig. 4. This map is to be compared with the $s = +1$ case shown in Fig. 1c and d. The main difference is that the negative divergent zone (blue in Fig. 4) is shifted downward for negative shear while it was shifted upward for positive shear. The consequence is that orientations that were departing from the vicinity of the ND fibre are returning back towards to it each time the sense of the shear is reversed. In this way, a good ND fibre can be maintained during ASR.

5. R value predictions

A systematic study has been carried out to evaluate the changes that take place in the R values after SR and ASR when the initial texture is the ideal ND fibre. The VPSC code was used for this purpose; the calculations were done for the textures that were modelled with the self-consistent model. The results obtained are displayed in Fig. 5.

The R value corresponding to the initial ideal ND fibre was 2.2 with in plane isotropy, which is expected. After SR to a strain of 1, the R values increased but in an anisotropic way as the obtained ND fibre was not uniform (see the texture in Fig. 2). This anisotropy remained valid also for ASR with a general small decrease of the R values for $s = 0.5$ and some more for $s = 1$. When the shear component was cyclic, this diminution of the R value was significantly smaller up to $s = \pm 1$. By increasing further the shear component, the R values decrease dramatically. Therefore, it can be concluded that an optimum limit of the shear component is $s = 1$ during which the high R values can still be maintained. Even better results were obtained when the shear component changes sign between passes. These predictions were actually confirmed by the experimental results that will be presented in the next section.

6. Experimental study

We have carried out experiments for the purpose of verifying the theoretical predictions presented above concerning the effect of alternating shear in ASR vs. monotonic shear in ASR. Although our experimental initial texture presented only a weak ND fibre, the tendencies in the texture variations and R value predictions should be similar as for a strong ND fibre–which was considered in the modelling in Section 5.

As-received hot-rolled 5.6 mm thick IF steel (Fe–0.0017C–0.05Mn–0.011P–0.005Si–0.023Al–0.021–Cr–0.052Ti–0.002 wt.%)

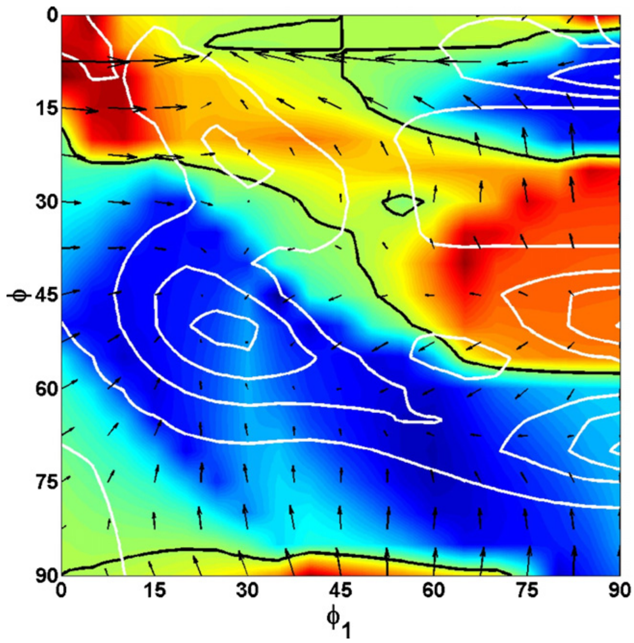

Fig. 4. The persistence map and the divergence quantity in the $\varphi_2 = 45°$ section of Euler space for negative shear during asymmetric rolling.

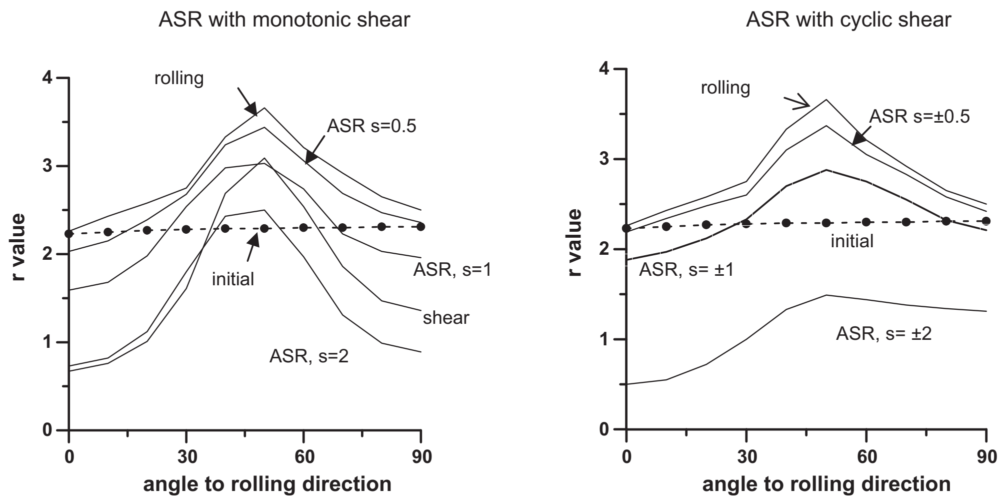

Fig. 5. Simulated *R* values obtained with the VPSC code from the textures modelled after SR and ASR.

Table 1
Deformation characteristics of IF steel sheet during cold rolling used in this study.

Strain	Units	Rolling pass number						Total
		1	2	3	4	5	6	
Reduction in thickness, Δh	[mm]	0.7	0.72	0.68	0.65	0.75	0.2	3.7
Elongation, h_n/h_{n-1}		1.143	1.172	1.194	1.228	1.357	1.105	2.947
Engineering strain[a], e	[%]	12.50	14.69	16.27	18.57	26.32	9.52	66.07
Equivalent von Mises strain[a], ε		0.1542	0.1835	0.2050	0.2372	0.3526	0.1156	1.25

[a] Extra shear strain introduced due to the asymmetry is not taken into account.

sheet was homogenized at 1050 °C during 1 h and cooled on air. Then, it was symmetrically or asymmetrically (one roll was idle) rolled at ambient temperature down to 1.9 mm in six passes with the same sequence of reductions per pass, see Table 1. The ASR rolling was done in monotonic (the idle roll was always on the same side of the sheet, ASRm) and reversal (the sheet was turned 180° around the rolling direction between the passes, ASRr) modes. The rolls diameters were 175 mm. There was no lubrication of the specimens during either SR or ASR rolling in order to increase the shear component.

Texture measurements were done on a GBC MMA X-ray diffractometer equipped with a Cu Kα anode; no symmetry conditions were imposed on the recalculated pole figures. Mechanical properties were determined in tensile tests on flat samples scaled as 1:2.5 from standard ASTM E8M-08. The samples were cut in 0°, 45°, and 90° with respect to the RD directions. The tests were done on an INSTRON 55R4505 machine with 10 kN load cell using a standard 10 mm extensometer. *R* values were measured posterior on the tensile deformed specimens, far from the fractured region (the tensile strains were relatively small because of the hardening of the sample due to rolling).

The measured textures are presented in Fig. 6 in the $\varphi_2 = 45°$ section of Euler space. As can be seen, a weak but ND-type fibre existed before ASR. After monotonic ASR, the ND fibre appears shifted down towards larger ϕ values, which agrees with the prediction presented in Section 4 above for continuous negative shear (see Fig. 4). When the direction of shear is reversed after each pass, then the texture presents a partial ND fibre and a pronounced shear component as well (Fig. 6). The relative amount of the shear component was not known in the ASR experiment but it could be estimated from finite element simulations to be between $s = \pm 1$ and $s = \pm 2$ (Orlov et al., 2010). The measured *R* values are summarized in Table 2.

Table 2 shows that the initial *R* value was relatively small and with some in plane anisotropy after symmetric rolling. The average

Table 2
R values measured after symmetric and asymmetric rolling.

Rolling	Direction	No	r	r_{aver}	$\bar{R}$	ΔR
SR	0°	1	0.99	1.04	0.99	-0.13
		2	1.10			
	45°	1	0.99	1.05		
		2	1.10			
	90°	1	0.64	0.81		
		2	0.98			
ASRm	0°	1	0.75	0.60	0.80	-0.28
		2	0.44			
	45°	1	1.07	0.94		
		2	0.82			
	90°	1	0.63	0.72		
		2	0.80			
ASRr	0°	1	1.06	1.08	1.08	0.07
		2	1.10			
	45°	1	1.29	1.05		
		2	0.82			
	90°	1	1.07	1.15		
		2	1.23			

R decreased after monotonic ASR and the anisotropy increased substantially which is represented by a ΔR value of −0.28. However, for ASR with alternating shear (ASRr), the *R* values increased and the planar anisotropy was low. These experimental results indicate that it is more beneficial to perform asymmetric rolling by alternating the shear direction. This reversal of the shear component can be done by rotating the sample around the RD direction after each pass (this was done in the present experiment) but the same result should be obtained without this rotation by making the upper or the bottom roll idle after each pass. In conclusion, the experimental results confirm the theoretical predictions.

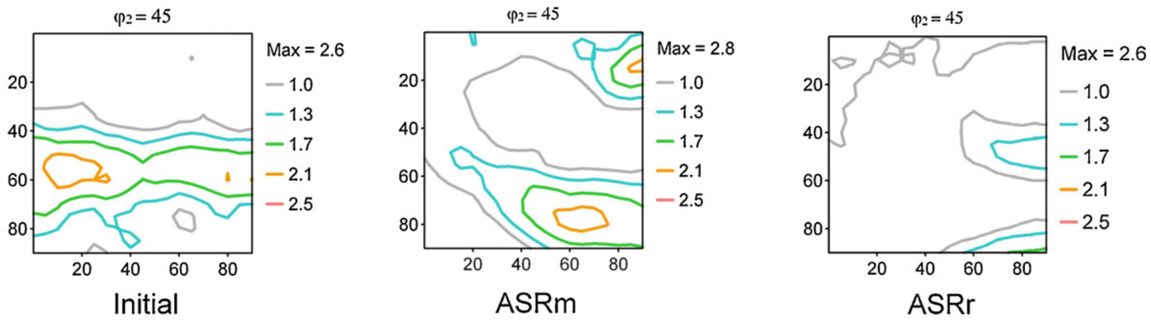

Fig. 6. Experimental initial and ASR textures in IF steel obtained with monotonic (ASRm) and cyclic (ASRr) shear.

7. Conclusions

From the present investigation, the following major conclusions can be drawn:

(1) A stability analysis carried out for asymmetric rolling in Euler space. It has been found that due to the shear component in ASR, the ND fibre is displaced in orientation space. This displacement is in the opposite direction when the shear component is reversed.
(2) Polycrystal simulations showed that the ND fibre can be maintained during ASR up to about a shear of $\gamma = 2$ during a rolling strain of $\varepsilon = 1$ when the VPSC model is used.
(3) Starting with an ideal ND fibre, the predicted R values in ASR are almost as high as for symmetric rolling if the shear component is not too high. An optimum value of $\gamma = \pm 1$ has been identified for $\varepsilon = 1$ rolling strain; below this limit, the R value decreases drastically.
(4) It was shown by simulations, that cyclic asymmetrical rolling (ASRr) leads to better R values than SR. Experimental work on IF steel confirmed this main finding.

Acknowledgements

This work was supported by a Linkage Industrial project of the Australian Research Council (LP0989455). B. Beausir thanks the Alexander von Humboldt Foundation for his research fellowship.

References

Apps, P.J., Heason, C.P., Prangnell, P.B., 2004. Ultrafine-grain structures produced by severe deformation processing. Mater. Sci. Forum 447–448, 423–428.
Arzaghi, M., Beausir, B., Tóth, L.S., 2009. Contribution of non-octahedral slip to texture evolution of fcc polycrystals in simple shear. Acta Mater. 57, 2440–2453.
Azushima, A., Kopp, R., Korhonen, A., Yang, D.Y., Micari, F., Lahoti, G.D., Groche, P., Yanagimoto, J., Tsuji, N., Rosochowski, A., Yanagida, A., 2008. Severe plastic deformation (SPD) processes for metals. CIRP Ann.: Manuf. Technol. 57, 716–735.
Baczynski, J., Jonas, J., 1998. Torsion textures produced by dynamic recrystallization in α-iron and two interstitial-free steels. Metall. Mater. Trans. A 29, 447–462.
Beausir, B., Biswas, S., Kim, D.I., Tóth, L.S., Suwas, S., 2009. Analysis of microstructure and texture evolution in pure magnesium during symmetric and asymmetric rolling. Acta Mater. 57, 5061–5077.
Beausir, B., Tóth, L.S., 2008. A new flow function to model texture evolution in symmetric and asymmetric rolling. In: Haldar, A., Suwas, S., Bhattacharjee, D. (Eds.), International Conference on Microstructure and Texture in Steels, MATS2008. Springer Verlag, Jamshedpur, India, pp. 415–420.
Beausir, B., Tóth, L.S., Bouaziz, O., 2005. Simulation of texture development of plane carbon steel in multipass rolling using analytical flow function. Mater. Sci. Forum 495–497, 1603–1608.
Beausir, B., Tóth, L.S., Neale, K.W., 2007. Ideal orientations and persistence characteristics of hexagonal close packed crystals in simple shear. Acta Mater. 55, 2695–2705.
Beygelzimer, Y., Orlov, D., Varyukhin, V., 2002. A new severe plastic deformation method: twist extrusion. In: Zhu, Y.T., Langdon, T.G., Mishra, R.S., Semiatin, S.L., Saran, M.J., Lowe, T.C. (Eds.), TMS Annual Meeting and Exhibition. TMS (The Minerals Metals & Materials Society), Seattle, Washington, USA, pp. 297–304.
Clément, A., Coulomb, P., 1979. Eulerian simulation of deformation textures. Scr. Metall. 13, 899–901.
Daniel, D., Jonas, J., 1990. Measurement and prediction of plastic anisotropy in deep-drawing steels. Metall. Mater. Trans. A 21, 331–343.
Dyja, H., Korczak, P., Pilarczyk, J.W., Grzybowski, J., 1994. Theoretical and experimental analysis of plates asymmetric rolling. J. Mater. Process Technol. 45, 167–172.
Gilormini, P., Tóth, L.S., Jonas, J.J., 1990. An analytic method for the prediction of ODFS with application to the shear of FCC polycrystals. Proc. R. Soc. Lond. Ser. A: Math. Phys. Sci. 430, 489–507.
Gorelik, V.S., Klimenko, I.V., 1997. Classification and analysis of processes of plate/strip rolling with asymmetric deformation zone. Russ. Metall., 34–42.
Hutchinson, J.W., 1976. Bounds and self-consistent estimates for creep of polycrystalline materials. Proc. R. Soc. Lond. A: Math. Phys. Sci. 348, 101–127.
Ji, Y.H., Park, J.J., 2009. Development of severe plastic deformation by various asymmetric rolling processes. Mater. Sci. Eng. A 499, 14–17.
Kocks, U.F., Mecking, H., 2003. Physics and phenomenology of strain hardening: the FCC case. Prog. Mater. Sci. 48, 171–273.
Lapovok, R., Tóth, L.S., Winkler, M., Semiatin, S.L., 2009. A comparison of continuous SPD processes for improving the mechanical properties of aluminum alloy 6111. J. Mater. Res. 24, 459–469.
Meyers, M.A., Mishra, A., Benson, D.J., 2006. Mechanical properties of nanocrystalline materials. Prog. Mater. Sci. 51, 427–556.
Molinari, A., Tóth, L.S., 1994. Tuning a self-consistent viscoplastic model by finite element results. I. Modeling. Acta Metall. Mater. 42, 2453–2458.
Montheillet, F., Gilormini, P., Jonas, J.J., 1985. Relation between axial stresses and texture development during torsion testing: a simplified theory. Acta Metall. Mater. 33, 705–717.
Orlov, D., Beygelzimer, Y., Synkov, S., Varyukhin, V., Tsuji, N., Horita, Z., 2009. Plastic flow, structure and mechanical properties in pure Al deformed by twist extrusion. Mater. Sci. Eng. A 519, 105–111.
Orlov, D., Lapovok, R., Tóth, L.S., Timokhina, I.B., Hodgson, P.D., Bhattacharjee, D., Haldar, A., 2010. Structure and mechanical properties of asymmetrically rolled IF steel sheet. Mater. Sci. Forum 654–656, 1255–1258.
Potapkin, V.F., Satonin, A.B., Dobronosov, Y.K., 1987. Deformation of metal in asymmetric rolling of thin strips. Russ. Metall., 62–66.
Richelsen, A.B., 1997. Elastic–plastic analysis of the stress and strain distributions in asymmetric rolling. Int. J. Mech. Sci. 39, 1199–1211.
Salganik, V.M., Pesin, A.M., 1997. Asimmetrichnaya tonkolistovaya prokatka: razvitie teorii, tekhnologii inovye resheniya (Asymmetric Thin Sheet Rolling: Development of the Theory and Technology and New Approaches). MISiS, Moscow.
Segal, V.M., Reznikov, V.I., Drobyshevkiy, A.E., Kopylov, V.I., 1981. Plastic metal working by simple shear. Russ. Metall. 99.
Takechi, H., 1994. Metallurgical aspects on interstitial free sheet steel from industrial viewpoints. ISIJ Int. 34, 1–8.
Tóth, L., Jonas, J., Daniel, D., Ray, R., 1990. Development of ferrite rolling textures in low- and extra low-carbon steels. Metall. Mater. Trans. A 21, 2985–3000.
Tóth, L.S., 2008. Simulation of persistence characteristics of textures during plastic deformation. In: Haldar, A., Suwas, S., Bhattacharjee, D. (Eds.), International Conference on Microstructure and Texture in Steels, MATS2008. Springer Verlag, Jamshedpur, India, pp. 225–246.
Tóth, L.S., Arzaghi, M., Fundenberger, J.J., Beausir, B., Bouaziz, O., Arruffat-Massion, R., 2009. Severe plastic deformation of metals by high-pressure tube twisting. Scr. Mater. 60, 175–177.
Tóth, L.S., Gilormini, P., Jonas, J.J., 1988. Effect of rate sensitivity on the stability of torsion textures. Acta Metall. Mater. 36, 3077–3091.
Tsuji, N., Saito, Y., Utsunomiya, H., Tanigawa, S., 1999. Ultra-fine grained bulk steel produced by accumulative roll-bonding (ARB) process. Scr. Mater. 40, 795–800.
Urabe, T., Jonas, J.J., 1994. Modeling texture change during recrystallization of an IF steel. ISIJ Int. 34, 435–442.
Valiev, R.Z., Langdon, T.G., 2006. Principles of equal-channel angular pressing as a processing tool for grain refinement. Prog. Mater. Sci. 51, 881–981.
Zhilyaev, A.P., Langdon, T.G., 2008. Using high-pressure torsion for metal processing: fundamentals and applications. Prog. Mater. Sci. 53, 893–979.